The Effect of Xuebijing on the Gut Microbiota and Metabolic of Heat 1 Stroke Rat 2

Qiang wen
Southern Medical University
Xuan He
General Hospital of Guangzhou Military Command
Yu Shao
General Hospital of Guangzhou Military Command
Lun Peng
Southern Medical University
Li Zhao
Guangzhou University of Chinese Medicine
Guo Pan
Southern Medical University
Lei Su (Slei_icu1@126.com)
Southern Medical University

Research Article

Keywords: gut microbiome, metabolites, heat stroke, Xuebijing, rat

Posted Date: February 1st, 2021

DOI: https://doi.org/10.21203/rs.3.rs-142370/v1

The effect of Xuebijing on the gut microbiota and metabolic of heat stroke rat

Qiang Wen [1,2], Xuan He [2], Yu Shao[3], Lun Hai Peng [1], li Yue Zhao [4], Guo Zhi Pan[1,2*],Lei Su[1,2*]

[1] The First Clinical Medical College, Southern Medical University, Guangzhou, 510515,China

[2] Department of ICU, General Hospital of Guangzhou Military Command, Guangzhou,510010, China

[3] Second Department of Internal Medicine for Cadres, General Hospital of Guangzhou Military Command, 510010, China

[4] Graduate School, Guangzhou University of Traditional Chinese Medicine, 510006, Guangzhou, China

*** Corresponding authors:**

Guo Zhi Pan (gzpzg@126.com),

Lei Su (Slei_icu1@126.com)

Keywords: gut microbiome, metabolites, heat stroke, Xuebijing, rat

Abstract

The goal of the present study was to evaluate the fecal microbiome and serum metabolites in Xuebijing (XBJ)-injected rats after heat stroke using 16S rRNA gene sequencing and gas chromatography-mass spectrometry (GC-MS) metabolomics. Eighteen rats were divided into the control group (CON), heat stroke group (HS), and XBJ group. The 16S rRNA gene sequencing results revealed that the abundance of Bacteroidetes was overrepresented in the XBJ group compared to the HS group, while Actinobacteria was underrepresented. Metabolomic profiling showed that the pyrimidine metabolism pathway, pentose phosphate pathway, and glycerophospholipid metabolism pathway were upregulated in the XBJ group compared to the HS group. Taken together, these results demonstrated that heat stroke not only altered the gut microbiome community structure of rats but also greatly affected metabolic functions, leading to gut microbiome toxicity.

Introduction

Heat stroke is a life-threatening syndrome induced by environmental or metabolic factors. Heat stroke causes body temperature dysregulation, sweat gland failure and electrolyte disturbances [1],

leading to debilitating central nervous system damage and the potential for the subsequent rapid development of cardiovascular dysfunction [2,3]. Body temperature continues to rise, cardiac output is difficult to maintain balance, induce cytotoxicity and inflammation, and ultimately lead to multiple organ failure [4-6].

The gastrointestinal mucosal barrier has the function of preventing harmful substances in the intestinal cavity from entering the blood circulation. When heatstroke occurs, intestinal blood loss, intestinal blood flow decreases, intestinal epithelial cell vitality decreases, and cell wall permeability increases [7]. In addition, the oxides and nitrosamines produced in the intestine can stimulate the cell membrane and destroy the tight junctions between cells. The endotoxins and potential pathogens in the intestine enter the blood, pass through the systemic circulation, and reach the liver. The liver's detoxification ability cannot meet the demand, leading to toxemia. Microbial products in the intestine will also be transferred to the systemic circulation [8]. The gastrointestinal microbiota is a collection of microorganisms that colonize the gastrointestinal tract, which have co-evolved inside humans and are considered to provide several mutually beneficial host functions [9], including digesting food components, synthesizing vitamins, antagonizing pathogens, detoxifying carcinogenic compounds, and releasing a variety of metabolites involved in the homeostatic balance achieved between microbiota and the host [10,11]. . However, other microorganisms can faster pro-inflammatory reactions, interfere with the energy metabolism of epithelial cells, cause severe heat stroke and destroy the epithelial barrier. Studies have found that the diversity and functions of the host microbial community can be changed according to changes in the host's diet or physiology [12,13]. Therefore, we believe that there is a close relationship between heatstroke and gut microbes.

Xuebijing (XBJ) injection is a traditional Chinese medicine consisting of Carthami flos, Paeoniae Radix Rubra, Chuanxiong Rhizoma, Salviae miltiorrhizae, and Angelicae Sinensis Radix. XBJ has two primary effects in the treatment of sepsis [14]. XBJ injection directly reduces damage to the vascular endothelium and inhibits the release of inflammatory factors, protecting multiple organs in heatstroke-affected animals, including the heart, liver, and kidneys. In addition, XBJ injection can prevent the translocation of bacteria and endotoxins by maintaining the structural integrity of the intestinal barrier and indirectly aids in reducing systemic inflammation [15]. Although XBJ likely as potential as an effective treatment for heatstroke, few studies have addressed the roles of XBJ in heat stroke. Additionally, the roles of XBJ in gastrointestinal disorders during heatstroke require further investigation. We hypothesized that XBJ is a protective agent that can attenuate gastrointestinal disorders during heat stroke by affecting the gut microbiome.

Therefore, in the present study, we used the classic severe heat stroke rat model to investigate the role of the gut microbiome and blood metabolites in heat stroke by comparing the effects of heat stress and XBJ during heat stroke.

RESULTS

General parameters

The results showed that compared to the CON group, body weight gain and body temperature increased after heat shock ($P < 0.05$), while no difference in body weight gain and body temperature was observed in the XBJ group ($P > 0.05$). The LPS content increased after heat shock ($P < 0.05$), and the use of XBJ inhibited the increase in LPS ($P < 0.05$) (Table 1).

Effect of XBJ on intestinal structure

Compared to the control group, the HS group had severe intestinal bleeding, and the symptoms were relieved after treatment with XBJ (Fig. 1A). Fig. 1B shows that the jejunum, ileum, cecum, and colon of rats in the HS group were severely damaged. After the injection of XBJ, the level of damage to each intestinal segment decreased. The colonic epithelial cells in the CON group were intact, with tight cell connections without gaps. In the HS group, the tight junctions between colonic epithelial cells were destroyed, the gaps widened, and the boundaries were obvious. Compared to the HS group, the space between colonic epithelial cells in the XBJ group became narrower, but the boundary was not obvious (Fig. 1C).

Effect of XBJ on the fecal microflora composition

A total of 1,364,540 high-quality 16S rRNA gene reads were obtained, with an average of 32,956 reads per sample. Following taxonomic assignment, 1401 OTUs were obtained (see Supplementary Table S1 online). To evaluate the differences in bacterial diversity between the two groups, sequences were aligned to estimate alpha diversity and beta diversity. No statistically significant differences were observed in the Chao1 index ($P = 0.74$), Goods coverage ($P = 0.44$), Shannon index ($P = 0.88$) or Simpson index ($P = 0.37$), whereas the Chao1 index in the XBJ group was higher than that in the HS group (Table 2). The Bray-Curtis PCoA plots revealed a separation of

the three groups (Fig. 2A). These results suggest that the diversity of gut microbiota could be strongly influenced by XBJ treatment.

The relative proportions of dominant taxa at the phylum level were assessed by microbial taxon assignment among the three groups. We observed considerable variability in gut microbiota across samples in each group. Six phyla were identified in each group. Firmicutes was the most predominant phylum, accounting for 69.71, 75.48 and 70.29% of the OTUs in the CON, HS and XBJ groups, respectively. In addition, Bacteroidetes was enriched in the XBJ and CON groups compared to the HS group (Fig. 2B). At the genus level, Prevotella_9 was observed to be less abundant in the HS group than in both the CON and XBJ groups (Fig. 2C). Considering that this discriminant analysis did not distinguish the predominant taxon, LEfSe was used to generate a cladogram to identify the specific bacteria associated with the XBJ group (Fig. 2D). Seven different genera were identified. Ruminococcaceae_UGG_013, Ruminiclostridium_5, Anaerofustis and Jeotgalicoccus were all significantly overrepresented in the CON group (all LDA scores (log10) > 3), whereas Bifidobacterium and Faecalibaculum were the most abundant microbiota in the HS group (all LDA scores (log10) > 3), and Shuttleworthia was the only genus enriched in the HS_XBJ group (all LDA scores (log10) > 3.5) (Fig. 1C). The relative abundances of the top 21 genera were further analyzed by heat map clustering analysis, and the results were consistent with the LEfSe results (Fig. 2E).

Multivariate statistical analysis and identification of serum metabolites

OPLS-DA is a multivariate statistical analysis tool used to identify differences in the biochemical compositions of metabolites to discriminate different groups. The score plot of the OPLS-DA in the negative mode [(R2X = 0.523, R2Y = 0.995, Q2 = 0.664 between CON and HS groups) and (R2X = 0.335, R2Y = 0.991, Q2 = 0.365 between XBJ and HS groups)] and the results of the OPLS-DA in the positive mode showed that the CON, HS and XBJ groups underwent significant metabolic changes [(R2X = 0.362, R2Y = 0.955, Q2 = 0.587 between CON and HS groups) and (R2X = 0.462, R2Y = 0.995, Q2 = 0.523 between XBJ and HS groups)] (see Supplementary Table S2 online). One hundred seventy metabolites in the negative mode and 260 metabolites in the positive mode were observed to differ in abundance between the CON and HS groups (see Supplementary Fig. S1 and S2 online). Moreover, the abundances of 67 metabolites in the negative mode and 106 metabolites in the positive mode were altered in the XBJ and HS groups (see Supplementary Fig. S3 and S4). Further analysis revealed that 17 metabolites identified in the negative mode were shared between the CON vs HS and XBJ vs HS comparisons, including 681 (cyanuric acid), 1539 (metaraminol), 1556

(vanillic acid), 1846 (acamprosate), 5822 (cis-9,10-epoxystearic acid), 5957 (eicosapentaenoic acid), 6148 (alprazolam), 6633 (D-lactose), 7289 [(3S,4S)-3-hydroxytetradecane-1,3,4-tricarboxylate], 8446 (ferulic acid), 8842 (thiamine monophosphate), 9428 (furcatin), 9530 (LDS-751), 9652 (sphingosine-1-phosphate), 10081 (clindamycin), 11130 (DAMGO), and 14061 (PG). Moreover, 45 common metabolites were identified in the positive mode between the CON vs HS and XBJ vs HS comparisons, including 42 (acrylamide), 176 (acrylamide), 704 (L-lysine), 731 (alpha-fluoro-beta-alanine), 801 (oxindole), 1098 (1,2-benzenedicarboxylic acid), 1148 (2-dimethylamino-5,6-dimethylpyrimidin-4-ol), 1291 (D-glucuronate), 1476 (2-dimethylamino-5,6-dimethylpyrimidin-4-ol), 1612 (L-arginine), 1632 (propionylglycine), 1869 (aceclidine), 2148 (IS), 2270 (methacholine), 2530 (talbutal), 2603 (ketorolac), 2769 (dimethyl sulfone), 3094 (L-histidinol phosphate), 3204 (thymidine), 3417 (2,4-dichloro-3-oxoadipate), 3565 (palmitic amide), 3571 (phosfolan), 3679 (Phe-Ala), 3707 (clofibrate), 4213 (triprolidine), 4595 (chlormezanone), 4784 (kaempferol), 5132 (phytosphingosine), 5135 (terodiline hydrochloride), 5407 (monomethyl glutaric acid), 5518 (parathion), 5662 (Oleic acid), 5695 (scopolamine), 5975 [(1x,2x)-cuaiacylglycerol 3-glucoside], 5992 (methyclothiazide), 6022 (norfloxacin), 6240 (cellulose), 7779 (2',3'-dideoxyadenosine-5-triphosphate), 8038 (sulfolithocholylglycine), 8248 (sulfolithocholylglycine), 8416 (sulfolithocholylglycine), 8484 (lupiwighteone hydrate 7-glucoside), 8750 (sulfolithocholylglycine), 9751 (goyaglycoside c), and 10347 (lycoperoside D).

Pathway analysis of metabolites

KEGG analysis was also used to identify the most crucial signal transduction pathway and biochemical metabolic pathway relevant to differential metabolites. The differential metabolites of the CON and HS groups were primarily enriched in the ascorbate and aldarate metabolic pathways (Fig. 3A, 3B). Different metabolites between the HS_XBJ and HS groups were distributed in the pyrimidine metabolism pathway, pentose phosphate pathway, and glycerophospholipid metabolism pathway (Fig. 3C, 3D).

DISCUSSION

After heat stroke, the intestine is the most vulnerable target organ [16]. Intestinal barrier dysfunction is related to the development of multiple organ dysfunction syndrome caused by trauma-hemorrhagic

shock [17]. Our results showed that the intestinal tract showed oozing blood and that the intestinal barrier was damaged after heat shock, indicating that heat shock is likely to cause trauma-hemorrhagic shock. The intestinal flora is also an important component of the intestinal barrier, and it forms an interdependent and interactive microecosystem with intestinal epithelial cells. Previous studies have shown that the intestinal flora contributes to the occurrence and development of a variety of metabolic syndrome diseases, such as obesity, diabetes and cardiovascular disease [18]. Therefore, it is important to elucidate the function of intestinal flora to treat intestinal injury caused by heat stroke. Metabolites are the media that connect microbes and the intestine, but there are few reports on the changes in the metabolism of intestinal substances caused by heat stroke.

Firmicutes and Bacteroidetes are the two primary phyla in the gut microbiota and are involved in lipid and bile acid metabolism to maintain energy balance in the body [19]. Bervoets et al. observed that compared to thin people, the relative abundance of Firmicutes is increased in the intestines of obese people, while that of Bacteroidetes is decreased [20]. In another study, Collado et al. observed that the relative abundance of Bacteroidetes in the gut of obese patients increases [21]. However, our findings contrast with the above findings, as the relative abundance of Bacteroidetes decreased with less body weight gain in the HS group. The gut microbes of 12 severely ill patients were evaluated in a previous study, and the results showed that the ratio of Bacteroidetes to Firmicutes was relatively stable in the 6 surviving patients, while that of Bacteroidetes to Firmicutes was higher than 10 or less than 0.10 in the other patients who died, indicating that the extreme imbalance of intestinal flora may affect the prognosis of critically ill patients [22]. The results obtained by Lankelma et al. also showed that the ratio of Bacteroidetes to Firmicutes in the guts of severely ill patients varied greatly compared with that of healthy people [23]. These findings may explain our findings reasonably well. At the genus level, the decrease in Prevotella-9 and Prevotella-1 in the HS group may be the primary reason for the decrease in Bacteroidetes microorganisms, as Prevotella-9 and Prevotella-1 are the dominant genera of Bacteroidetes. Prevotella is the primary fiber-degrading genus in the in the phylum Bacteroidetes. The decrease in Prevotella-9 and Prevotella-1 indicated that the fiber digestion ability was weakened in the HS group, which may have affected the energy supply. In addition, members of the phyla Actinobacteria and Proteobacteria were also the primary dominant bacteria in the guts of rats. Compared to the control group, members of both phyla increased after heat shock. The phylum Proteobacteria was previously reported to be the primary source of various genes involved in carbon metabolism and the biosynthesis of unique secretion systems. Moreover, the phylum Proteobacteria includes many pathogens, such as *Escherichia coli*, *Salmonella*, *Vibrio cholerae*, and *Helicobacter pylori*, which cause intestinal inflammation and damage to the intestines [24]. An increased abundance

of Proteobacteria and a decreased abundance of Bacteroidetes was observed in the guts of patients with kwashiorkor [25]. The alterations in Proteobacteria and Bacteroidetes abundances observed in the present study were similar to those observed in the above study, indicating that heat stroke may cause malnutrition in rats. With XBJ injection after heat shock, the proportion of Bacteroidetes was close to that of the CON group, while the proportion of Proteobacteria was close to that of the HS group, indicating that XBJ may promote Bacteroidetes proliferation but may have no such effect on Proteobacteria. The abundance of the Actinobacteria phylum increased in the HS group, but the abundance of *Roseburia*, a member of the phylum Actinobacteria, decreased. Members of the genus *Roseburia* can ferment carbohydrates into butyric acid. In a previous study, *Roseburia* was transplanted into the intestine of apolipoprotein E-deficient mice, and the results showed that systemic inflammation was relieved, the risk of atherogenesis was reduced, fatty acid utilization was accelerated, and glycolysis was slowed [26]. In addition, the removal of butyric acid-producing bacteria often induces the overexpression of nitric oxide synthase type 2 and the production of nitrate, which eventually leads to the proliferation of Enterobacteriaceae in the Proteobacteria phylum [26]. In the present study, we identified two bacterial biomarker genera in the HS group, namely, *Bifidobacterium* and *Faecalibaculum*, by LEfSe analysis. *Bifidobacterium* belongs to the Actinobacteria phylum and improves the infection fighting ability of the intestinal mucosa by producing antibodies and cytokines [27]. Compared to patients with metabolic disorders, *Bifidobacterium* is richer and has a heritability of up to 45.7% in the intestines of healthy subjects [28]. Inconsistent with the results of the above study, the abundance of *Bifidobacterium* increased significantly after heat shock in the present study. In an experiment assessing alcohol damage to the intestine, and the abundance of *Bifidobacterium* was observed to increase [29]. *Faecalibaculum* belongs to the phylum Firmicutes and is involved in inflammation regulation and lipid metabolism [30]. When feeding mice a diet without aromatic hydrocarbon ligands, the addition of *Faecalibaculum* can increase intestinal IgA levels [31]. Moreover, *Faecalibaculum* can regulate symbiotic probiotics and improve the energy metabolism pathways, such as those associated with short-chain fatty acids, carbohydrates, and amino acids [32]. The increase in *Bifidobacterium* and *Faecalibaculum* after heat shock may be related to the self-repair of intestinal damage, but further proof is needed to assess this possibility.

Vitamin C (Vc), also called ascorbic acid, is a polyhydroxy compound that easily undergoes oxidative dehydrogenation reactions. Vc participates in the synthesis and decomposition of many important metabolites [33]. In the present study, the ascorbic acid and aldonic acid metabolic pathways were observed to be downregulated after heat shock, indicating that heat shock would cause a decrease in Vc. The results of a previous study showed that Vc is highly effective in treating sepsis patients

with a body temperature ≥37.1°C and white blood cell count ≥15.0 1000/mm^3, indicating that Vc is associated with fever and high inflammation [34]. Vc not only inhibits the expression of pro-inflammatory cytokines but also directly eliminates reactive oxygen species, thereby maintaining cortical barrier function, which indicates that intestinal injury in the heat shock group may be related to a decrease in the Vc content [35]. In patients with septic shock, increasing the clearance rate of thiamine and lactic acid can greatly reduce mortality, showing that thiamine and Vc can alleviate the damage caused by oxidative stress [36]. The findings of such studies provide more possibilities for Vc treatment in patients with sepsis [37]. Compared to that observed in the HS group, the metabolite glucuronate was significantly higher in the HS_XBJ group. Glucuronate is related to anticoagulation, indicating that XBJ can increase the production of Vc and promote blood coagulation. It has been reported that an impaired intestinal barrier can lead to interruption of oxygen and nutrient supplies, which is the primary cause of metabolic changes in specific tissues [38]. Therefore, we hypothesize that heat shock may disrupt those changes that are primarily used to compensate for intestinal dysfunction. The results showed that after the injection of XBJ, the pentose phosphate pathway metabolic pathway was significantly upregulated in the intestinal tract of heat shock-affected rats, especially the level of 5-phosphate ribose, which increased significantly. Ribose 5-phosphate plays a crucial role in nucleotide and nucleic acid synthesis [39]. In the pentose phosphate pathway, ribose 5-phosphate can be isomerized with 5-ribose by the action of 5-ribose ribose isomerase [40,41]. Under the action of trans ketolase, 5-phosphate ribose and 5-xylulose phosphate form glyceraldehyde 3-phosphate. Glyceraldehyde 3-phosphate can also be converted to triose phosphate isomerase. Therefore, the increase in the content of ribose 5 phosphate indicates that the pentose phosphate pathway may alleviate the gut damage caused by heat shock. The enhancement of the pentose phosphate pathway can increase the synthesis of reducing metabolites in cells, such as NADPH [42]. At the same time, 5-phosphate ribose and NADPH are the primary sources of rapid cell growth [43]. Sphingomyelin is an important part of cell membrane lipids and participates in a variety of cell signaling pathways. Sphingosine 1-phosphate (S1P) is one of the metabolites of sphingomyelin, a natural lysophosphatidic with important biological activity, which is involved in many physiological processes, such as cell growth, proliferation, migration, cytoskeleton remodeling and lymphocyte transport [44]. S1P is converted from sphingosine through sphingosine kinase and has the effect of preventing oxidative damage [45]. In the present study, the S1P content in the HS group was significantly increased and was significantly reduced in the XBJ group. In addition, phosphatidylcholine is the primary component of low-density lipoprotein and is related to the metabolism of polyunsaturated fatty acids and sphingomyelin [46,47]. After injection with XBJ, the level of phosphatidylcholine decreased, and the

content of 1-acyl-sn-glycero-3-phosphocholine increased. Therefore, it is speculated that XBJ can protect intestinal health by inhibiting the sphingolipid metabolism pathway in heat shock-affected rats.

In summary, heat shock significantly modified the structure and composition of the gut bacteria in rats. In the present study, we demonstrated heat shock-induced microbial disorders and the dysregulation of microbial metabolites. The results showed that the abundance of Bacteroidetes decreased and the abundance of Actinobacteria increased after heat shock, while the abundance of both phyla in the XBJ injection group was consistent with that of the control group. At the genus level, heat shock inhibits the proliferation of the Prevotella-9 and Prevotella-1 genera, but XBJ can promote their reproduction. Furthermore, we demonstrated the capabilities of a nontargeted GC-MS-based metabolomics approach to successfully identify 170 different metabolites between the CON and HS groups and 37 different metabolites between HS and XBJ groups.

Materials and Methods

Animals and Reagents

The experimental procedures were approved by Ethics Committee of the General Hospital of Guangzhou Military Command (No.2019090201) and performed in accordance with the ARRIVE guideline and the American Physiological Society's guiding principles for research involving animals and also adhered to the Guide for the Care and Use of Laboratory Animals. Adult 7-week-old male Sprague-Dawley rats (n=18, body weights 230~250 g)were purchased from the Central Animal Breeding House of Xi'an Jiaotong University (Xi'an, Shaanxi, China). The rats were housed at an ambient temperature of 20±2°C, a relative humidity of 50±10% and a 12 h light/dark cycle for 1 week prior to the start of the experiments. Pellet rat feed and tap water were available ad libitum.

Heat stroke induction

At the time of the beginning of form experiments, all rats were randomly divided into three groups: the sham control group (CON; n=6), model heat stroke group (HS; n=6), and drug treatment group (XBJ, n=6) groups. The groups had body weights of 238.0 ±2.3 g , 240 ±1.8 g and 237 ±1.9 g, respectively (mean ± SEM). Heat stroke was induced by placing rats into a floor-standing incubator (Thermo Scientific, Ashville, NC) preset to 42±0.2°C for 70 min. Twenty minutes after the 70-min heat stress treatment, all rats exhibited heat stroke reactions characterized by excessive rectal

hyperthermia (~42°C) [48]. The CON group animals were exposed to the same experimental conditions at 20±2°C.

Drug treatment and experimental procedure

XBJ was purchased from Tianjin Chase Sun Pharmaceutical Co., Ltd. (Tianjin, China) and stored at 4°C in the dark. Immediately following the exposure, the rats in the CON and HS groups received an intravenous injections of normal saline 4 (mL/kg body weight) via the femoral vein. The rats in the XBJ group received XBJ (4 mL/kg body weight) after the termination of heat stress once per day for 3 consecutive days. The body weight and rectal temperature of the rats were measured at the end of the formal experiment.

Sample collection

Colon tissues, fecal pellets and serum were collected after euthanasia.

Fecal pellets were placed in sterile conical tubes and immediately frozen at -80°C for further microbial community analysis. Serum was obtained by centrifugation of the blood at 3000 rpm for 15 min in a refrigerated centrifuge and then immediately stored at -80°C [49]. Lipopolysaccharide (LPS) levels were then measured with appropriate ELISA kits (MP Biomedicals, Santa Ana, CA, USA).

HE staining of tissue samples

Colon tissues were washed with cold phosphate buffered saline (PBS pH 7.4 and 0.01 mol/L) and immersed in 10% neutral formalin fixation solution. After dehydration and clearing, the tissues were immersed in wax and then cut into 5-8-micron-thick sections, which were then dewaxed and stained with HE.

Electron microscopy

Tissue samples were fixed in 2.5% glutaraldehyde and Hanks' balanced salt solution (pH= 7.0) at 4°C for 2 h. Subsequently, the tissues were postfixed in osmium tetroxide solution (1% OsO4 in Hanks' solution) at 4°C for 2 h and block stained with 2% uranyl acetate buffer at 40°C for 1 h before being dehydrated in ethanol and acetone and embedded in paraffin. Ultrathin tissue sections were obtained using an LKB-8800 ultramicrotome (LKB, Sweden) and were stained with uranyl acetate and lead citrate. A JEM-100C microscope (JEOL, Tokyo, Japan) was used to examine the tissue sections [50].

Fecal DNA extraction for microbiome analysis

Fecal genomic DNA was extracted using a QIAamp DNA Stool Mini kit (Qiagen, Hilden, Germany) according to the manufacturer's guidelines. The concentration and purity of DNA were determined using a NanoDrop 2000 UV-Vis spectrophotometer (Thermo Scientific, Wilmington, DE, USA), and DNA quality was assessed by 1% agarose gel electrophoresis. The extracted DNA was stored at -20°C for subsequent processing.

The amplicon library was constructed by amplifying the V3/V4 region of the 16S rRNA gene using the primer pair 338F_806R (338F: 5'-ACTCCTACGGGAGGCAGCAG-3', 806R: 5'-GGACTACHVGGGTWTCTAAT-3'). PCR amplification was performed using a GeneAmp 9700 thermocycler (ABI, USA) with TransStart FastPfu DNA Polymerase AP22102 under the following conditions: 95°C for 5 min followed by 30 cycles of 94°C for 30 s, 55°C for 30 s, and 72°C for 60 s, with a final extension step at 72°C for 8 min [51].

The PCR products were quantified using QuantiFluor™-ST (Promega, USA) according to the manufacturer's protocol. Purified DNA samples were sequenced using an Illumina MiSeq. High-quality filtering of the raw tags was conducted to acquire clean tags using QIIME (Version 1.8.0, http://qiime.org/). The filtered sequences were then clustered into operational taxonomic units (OTUs) according to representative sequences using Usearch (version 11.0, http://drive5.com/uparse/) and classified against the Greengenes Database (http://greengenes.secondgenome.com/) with a 97% sequence similarity threshold [52]. Bacterial analysis of Bray-Curtis dissimilarities calculated according to the altered abundances of gut microbiota was performed using R (version 4.0.2, https://www.r-project.org/) with the 'vegan' package.

Blood sample preparation for UPLC-MS analysis

Serum metabolites were analyzed using untargeted metabolomics via UPLC-–HDMS. After the serum samples had completely thawed at 4°C, 200 μL of each sample was transferred into 1.5-mL centrifuge tubes, to which 800 μL of methanol (precooled at -20°C) was added. The tubes were vortexed for 60 s using a MixStar (QL-866, Vortex Mixer) and then centrifuged for 10 min at 12,000 rpm and 4°C. The supernatant from each tube was transferred into another 1.5-mL centrifuge tube, and the samples were blow-dried by vacuum. To dissolve the samples, 300 μL of a methanol aqueous solution (4:1, 4°C) was added, and the samples were filtered through a 0.22-μm membrane (0.22-μm PTFE, Jin Teng) to obtain the prepared sample extracts for LC-MS [53].

The samples were analyzed via ultra-high performance liquid tandem chromatography quadrupole time of flight mass spectrometry (UHPLC-QTOFMS), which involved the use of an Agilent 1290 Infinity ultrahigh-performance liquid chromatograph and an Agilent 6538 UHD and Accurate-Mass Q-TOF mass spectrometer with an ACQUITY UPLC®HSS T3 column (2.1×100 mm, 2.5 μm). The original data were transformed using Agilent MassHunter Qualitative Analysis B.04.00 (Agilent Technologies, USA). The processed data set was then entered into the SIMCA-P software package (v13.0, Umetrics, Umeå, Sweden). The normalized data were then used to perform principal component analysis (PCA) and orthogonal partial least squares-discriminate analysis (OPLS-DA) [49].

Statistical analysis

Statistical analyses were performed using GraphPad Prism version 8.0. All data are presented as the means ± SEMs. Multiple comparisons were analyzed using one-way ANOVA. Statistical significance was defined at $P \leq 0.05$.

Author contributions

G.Z.P. and L.S. designed the study. Q.W. and X.H. performed the research. Y.S., L.H.P. and L.Y.Z. collected the samples. Q.W. analyzed the data and wrote the manuscript. All the authors contributed to the article and approved the submitted version.

Funding

This project was financially supported by the National Natural Science Foundation of China (No. 81873116, 81673835), the China Postdoctoral Science Foundation (No. 2018M630464), the Natural Science Foundation of Guangdong Province of China (No. 2018A0303130319), the Science and Technology Program of Guangzhou of China (No. 201904010426) and the Medical Science and Technology Research Foundation of Guangdong Province of China (No. B2018075).

Acknowledgments

The authors wish to thank Xi'an Dongao Biotechnology Co., Ltd., for the fruitful discussions and their sequencing service support.

Conflict of interest

The authors declare that the research was conducted in the absence of any commercial or financial relationships that could be construed as a potential conflict of interest.

References

1 Leon, L. R. & Bouchama, A. Heat stroke. *Compr Physiol* **5**, 611-647, doi:10.1002/cphy.c140017 (2015).

2 Dehbi, M. *et al.* Hsp-72, a candidate prognostic indicator of heatstroke. *Cell Stress Chaperones* **15**, 593-603, doi:10.1007/s12192-010-0172-3 (2010).

3 Yang, Y. L. & Lin, M. T. Heat shock protein expression protects against cerebral ischemia and monoamine overload in rat heatstroke. *Am J Physiol* **276**, H1961-1967, doi:10.1152/ajpheart.1999.276.6.H1961 (1999).

4 Gauer, R. & Meyers, B. K. Heat-Related Illnesses. *Am Fam Physician* **99**, 482-489 (2019).

5 Leon, L. R. & Helwig, B. G. Role of endotoxin and cytokines in the systemic inflammatory response to heat injury. *Front Biosci (Schol Ed)* **2**, 916-938, doi:10.2741/s111 (2010).

6 Lim, C. L. Heat Sepsis Precedes Heat Toxicity in the Pathophysiology of Heat Stroke-A New Paradigm on an Ancient Disease. *Antioxidants (Basel)* **7**, doi:10.3390/antiox7110149 (2018).

7 Ye, N., Yu, T., Guo, H. & Li, J. Intestinal Injury in Heat Stroke. *J Emerg Med* **57**, 791-797, doi:10.1016/j.jemermed.2019.08.033 (2019).

8 Wells, J. M. *et al.* Homeostasis of the gut barrier and potential biomarkers. *Am J Physiol Gastrointest Liver Physiol* **312**, G171-G193, doi:10.1152/ajpgi.00048.2015 (2017).

9 Thursby, E. & Juge, N. Introduction to the human gut microbiota. *Biochem J* **474**, 1823-1836, doi:10.1042/BCJ20160510 (2017).

10 Patterson, E. *et al.* Gut microbiota, obesity and diabetes. *Postgrad Med J* **92**, 286-300, doi:10.1136/postgradmedj-2015-133285 (2016).

11 Belkaid, Y. & Harrison, O. J. Homeostatic Immunity and the Microbiota. *Immunity* **46**, 562-576, doi:10.1016/j.immuni.2017.04.008 (2017).

12 Song, M., Garrett, W. S. & Chan, A. T. Nutrients, foods, and colorectal cancer prevention. *Gastroenterology* **148**, 1244-1260 e1216, doi:10.1053/j.gastro.2014.12.035 (2015).

13 Shoaie, S. *et al.* Quantifying Diet-Induced Metabolic Changes of the Human Gut Microbiome. *Cell Metab* **22**, 320-331, doi:10.1016/j.cmet.2015.07.001 (2015).

14 Chen, X. *et al.* Anti-sepsis protection of Xuebijing injection is mediated by differential regulation of pro- and anti-inflammatory Th17 and T regulatory cells in a murine model of

polymicrobial sepsis. *J Ethnopharmacol* **211**, 358-365, doi:10.1016/j.jep.2017.10.001 (2018).

15 Li, T. *et al.* Xuebijing Injection Alleviates Pam3CSK4-Induced Inflammatory Response and Protects Mice From Sepsis Caused by Methicillin-Resistant Staphylococcus aureus. *Front Pharmacol* **11**, 104, doi:10.3389/fphar.2020.00104 (2020).

16 MacFie, J. *et al.* Gut origin of sepsis: a prospective study investigating associations between bacterial translocation, gastric microflora, and septic morbidity. *Gut* **45**, 223-228, doi:10.1136/gut.45.2.223 (1999).

17 Kwon, J. *et al.* Metabolomics approach for the discrimination of raw and steamed Gastrodia elata using liquid chromatography quadrupole time-of-flight mass spectrometry. *J Pharm Biomed Anal* **94**, 132-138, doi:10.1016/j.jpba.2014.01.032 (2014).

18 Swidsinski, A. *et al.* Comparative study of the intestinal mucus barrier in normal and inflamed colon. *Gut* **56**, 343-350, doi:10.1136/gut.2006.098160 (2007).

19 Turnbaugh, P. J. *et al.* An obesity-associated gut microbiome with increased capacity for energy harvest. *Nature* **444**, 1027-1031, doi:10.1038/nature05414 (2006).

20 Bervoets, L. *et al.* Differences in gut microbiota composition between obese and lean children: a cross-sectional study. *Gut Pathog* **5**, 10, doi:10.1186/1757-4749-5-10 (2013).

21 Collado, M. C., Isolauri, E., Laitinen, K. & Salminen, S. Distinct composition of gut microbiota during pregnancy in overweight and normal-weight women. *Am J Clin Nutr* **88**, 894-899, doi:10.1093/ajcn/88.4.894 (2008).

22 Ojima, M. *et al.* Metagenomic Analysis Reveals Dynamic Changes of Whole Gut Microbiota in the Acute Phase of Intensive Care Unit Patients. *Dig Dis Sci* **61**, 1628-1634, doi:10.1007/s10620-015-4011-3 (2016).

23 Lankelma, J. M. *et al.* Critically ill patients demonstrate large interpersonal variation in intestinal microbiota dysregulation: a pilot study. *Intensive Care Med* **43**, 59-68, doi:10.1007/s00134-016-4613-z (2017).

24 Bradley, P. H. & Pollard, K. S. Proteobacteria explain significant functional variability in the human gut microbiome. *Microbiome* **5**, 36, doi:10.1186/s40168-017-0244-z (2017).

25 Stokke, R. *et al.* Functional interactions among filamentous Epsilonproteobacteria and Bacteroidetes in a deep-sea hydrothermal vent biofilm. *Environ Microbiol* **17**, 4063-4077, doi:10.1111/1462-2920.12970 (2015).

26 Kasahara, K. *et al.* Interactions between Roseburia intestinalis and diet modulate atherogenesis in a murine model. *Nat Microbiol* **3**, 1461-1471, doi:10.1038/s41564-018-0272-x (2018).

27 Rizzatti, G., Lopetuso, L. R., Gibiino, G., Binda, C. & Gasbarrini, A. Proteobacteria: A

Common Factor in Human Diseases. *Biomed Res Int* **2017**, 9351507, doi:10.1155/2017/9351507 (2017).

28 Lim, M. Y. *et al.* The effect of heritability and host genetics on the gut microbiota and metabolic syndrome. *Gut* **66**, 1031-1038, doi:10.1136/gutjnl-2015-311326 (2017).

29 Litwinowicz, K., Choroszy, M. & Waszczuk, E. Changes in the composition of the human intestinal microbiome in alcohol use disorder: a systematic review. *Am J Drug Alcohol Abuse* **46**, 4-12, doi:10.1080/00952990.2019.1669629 (2020).

30 Zhan, Z. L. *et al.* [Study of genuineness based on changes of ancient herbal origin--taking Astragalus membranaceus and Salvia miltiorrhiza as examples]. *Zhongguo Zhong Yao Za Zhi* **41**, 3202-3208, doi:10.4268/cjcmm20161714 (2016).

31 Cox, L. M. *et al.* Description of two novel members of the family Erysipelotrichaceae: Ileibacterium valens gen. nov., sp. nov. and Dubosiella newyorkensis, gen. nov., sp. nov., from the murine intestine, and emendation to the description of Faecalibaculum rodentium. *Int J Syst Evol Microbiol* **67**, 1247-1254, doi:10.1099/ijsem.0.001793 (2017).

32 Ke, X. *et al.* Synbiotic-driven improvement of metabolic disturbances is associated with changes in the gut microbiome in diet-induced obese mice. *Mol Metab* **22**, 96-109, doi:10.1016/j.molmet.2019.01.012 (2019).

33 Marik, P. E. Hydrocortisone, Ascorbic Acid and Thiamine (HAT Therapy) for the Treatment of Sepsis. Focus on Ascorbic Acid. *Nutrients* **10**, doi:10.3390/nu10111762 (2018).

34 Litwak, J. J., Cho, N., Nguyen, H. B., Moussavi, K. & Bushell, T. Vitamin C, Hydrocortisone, and Thiamine for the Treatment of Severe Sepsis and Septic Shock: A Retrospective Analysis of Real-World Application. *J Clin Med* **8**, doi:10.3390/jcm8040478 (2019).

35 Ettarh, R. R., Sofola, O. A. & Adigun, S. A. Role of the endothelium in the vascular effects of vitamin C in rats. *Pathophysiology* **9**, 97-101, doi:10.1016/s0928-4680(02)00077-9 (2003).

36 de Andrade, J. A. A. *et al.* The effect of thiamine deficiency on inflammation, oxidative stress and cellular migration in an experimental model of sepsis. *J Inflamm (Lond)* **11**, 11, doi:10.1186/1476-9255-11-11 (2014).

37 Kim, W. Y. *et al.* Combined vitamin C, hydrocortisone, and thiamine therapy for patients with severe pneumonia who were admitted to the intensive care unit: Propensity score-based analysis of a before-after cohort study. *J Crit Care* **47**, 211-218, doi:10.1016/j.jcrc.2018.07.004 (2018).

38 Kinross, J. M. *et al.* Global metabolic phenotyping in an experimental laparotomy model of surgical trauma. *J Proteome Res* **10**, 277-287, doi:10.1021/pr1003278 (2011).

39 Rupani, B. *et al.* Relationship between disruption of the unstirred mucus layer and intestinal restitution in loss of gut barrier function after trauma hemorrhagic shock. *Surgery* **141**, 481-489, doi:10.1016/j.surg.2006.10.008 (2007).

40 Wang, Y., Jones, M. K., Xu, H., Ray, W. K. & White, R. H. Mechanism of the Enzymatic Synthesis of 4-(Hydroxymethyl)-2- furancarboxaldehyde-phosphate (4-HFC-P) from Glyceraldehyde-3-phosphate Catalyzed by 4-HFC-P Synthase. *Biochemistry* **54**, 2997-3008, doi:10.1021/acs.biochem.5b00176 (2015).

41 Grochowski, L. L., Xu, H. & White, R. H. Ribose-5-phosphate biosynthesis in Methanocaldococcus jannaschii occurs in the absence of a pentose-phosphate pathway. *J Bacteriol* **187**, 7382-7389, doi:10.1128/JB.187.21.7382-7389.2005 (2005).

42 Sun, S., Hu, F., Wu, J. & Zhang, S. Cannabidiol attenuates OGD/R-induced damage by enhancing mitochondrial bioenergetics and modulating glucose metabolism via pentose-phosphate pathway in hippocampal neurons. *Redox Biol* **11**, 577-585, doi:10.1016/j.redox.2016.12.029 (2017).

43 Tsouko, E. *et al.* Regulation of the pentose phosphate pathway by an androgen receptor-mTOR-mediated mechanism and its role in prostate cancer cell growth. *Oncogenesis* **3**, e103, doi:10.1038/oncsis.2014.18 (2014).

44 Bandhuvula, P. *et al.* S1P lyase: a novel therapeutic target for ischemia-reperfusion injury of the heart. *Am J Physiol Heart Circ Physiol* **300**, H1753-1761, doi:10.1152/ajpheart.00946.2010 (2011).

45 Vazquez-de-Lara, L. G. *et al.* Phosphatidylethanolamine Induces an Antifibrotic Phenotype in Normal Human Lung Fibroblasts and Ameliorates Bleomycin-Induced Lung Fibrosis in Mice. *Int J Mol Sci* **19**, doi:10.3390/ijms19092758 (2018).

46 Mika, A. *et al.* Decreased Triacylglycerol Content and Elevated Contents of Cell Membrane Lipids in Colorectal Cancer Tissue: A Lipidomic Study. *J Clin Med* **9**, doi:10.3390/jcm9041095 (2020).

47 Mrnka, L., Novakova, O., Novak, F., Tvrzicka, E. & Pacha, J. Low-salt diet alters the phospholipid composition of rat colonocytes. *Physiol Res* **49**, 197-205 (2000).

48 Lin, X. *et al.* Myricetin against myocardial injury in rat heat stroke model. *Biomed Pharmacother* **127**, 110194, doi:10.1016/j.biopha.2020.110194 (2020).

49 Yu, M. *et al.* Variations in gut microbiota and fecal metabolic phenotype associated with depression by 16S rRNA gene sequencing and LC/MS-based metabolomics. *J Pharm Biomed Anal* **138**, 231-239, doi:10.1016/j.jpba.2017.02.008 (2017).

50 Markov, A. G. *et al.* Cholera toxin perturbs the paracellular barrier in the small intestinal epithelium of rats by affecting claudin-2 and tricellulin. *Pflugers Arch* **471**, 1183-1189, doi:10.1007/s00424-019-02294-z (2019).

51 Yu, L., Wang, L., Yi, H. & Wu, X. Beneficial effects of LRP6-CRISPR on prevention of alcohol-related liver injury surpassed fecal microbiota transplant in a rat model. *Gut Microbes* **11**, 1015-1029, doi:10.1080/19490976.2020.1736457 (2020).

52 DeSantis, T. Z. *et al.* Greengenes, a chimera-checked 16S rRNA gene database and workbench compatible with ARB. *Appl Environ Microbiol* **72**, 5069-5072, doi:10.1128/AEM.03006-05 (2006).

53 Abobo, C. V. *et al.* LC-MS/MS determination of etravirine in rat plasma and its application in pharmacokinetic studies. *J Chromatogr B Analyt Technol Biomed Life Sci* **878**, 3181-3186, doi:10.1016/j.jchromb.2010.09.016 (2010).

Figure legends

(1)

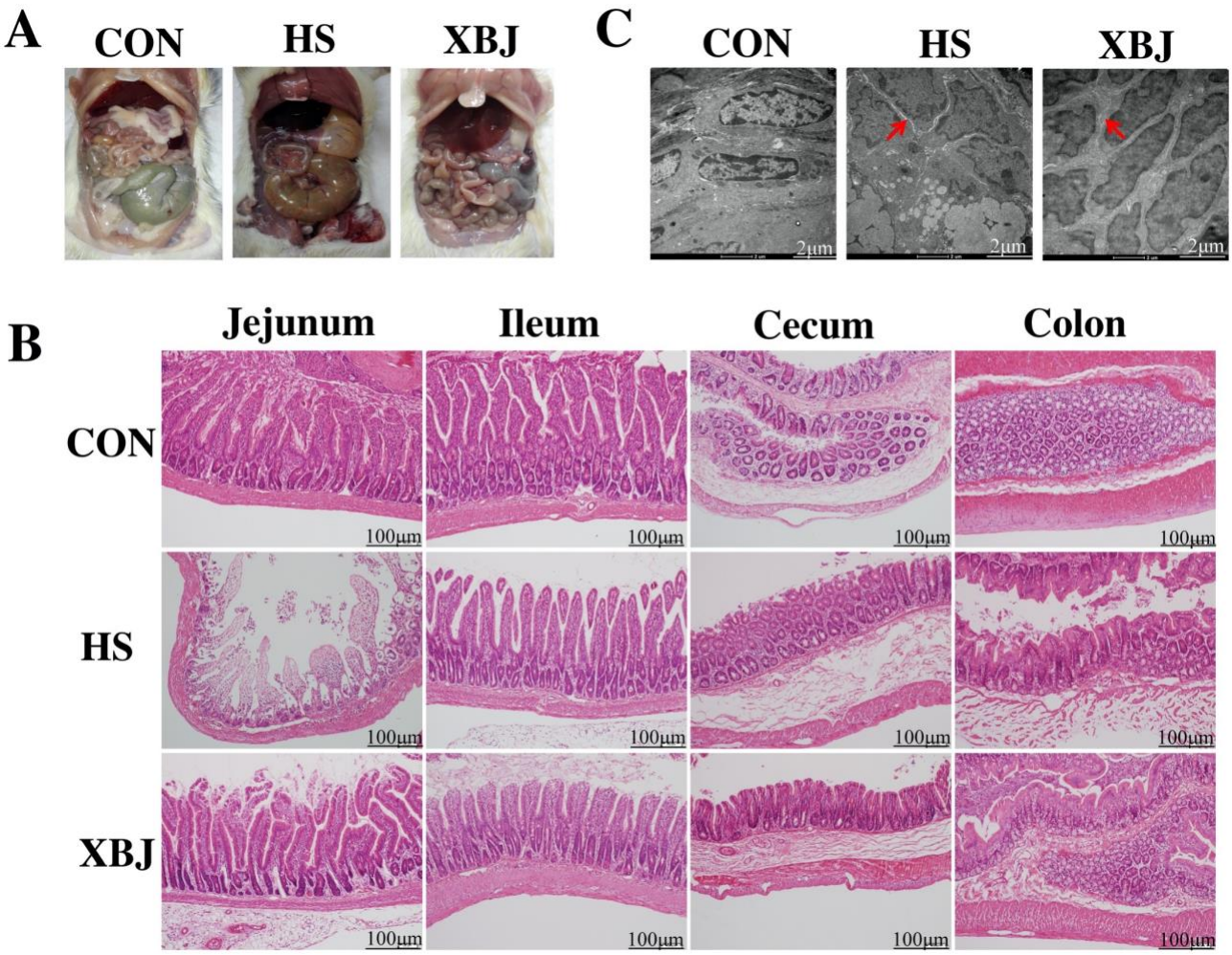

Figure 1. Intestinal structure. (A) Rat anatomy. (B) HE staining of different intestinal segments, including the jejunum, ileum, cecum and colon (40×). (C) Electron microscopy of the colon (8200×). Effect of XBJ on bacterial diversity in fecal microbiota

(2)

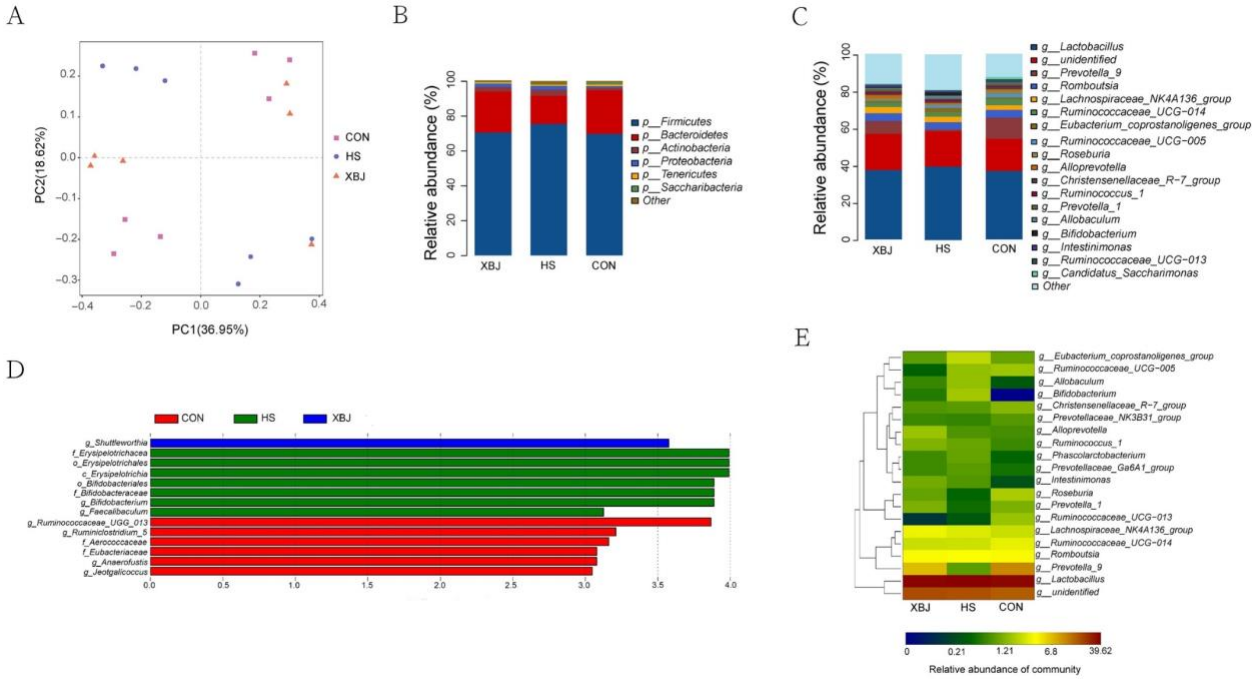

Figure 2. Intestinal microbiota. (A) Bray-Curtis PCoA plots. (B) Bar plot at the phylum level. (C) Bar plot at the genus level. (D) LEfSe score. (E) Heatmap at the genus level.

(3)

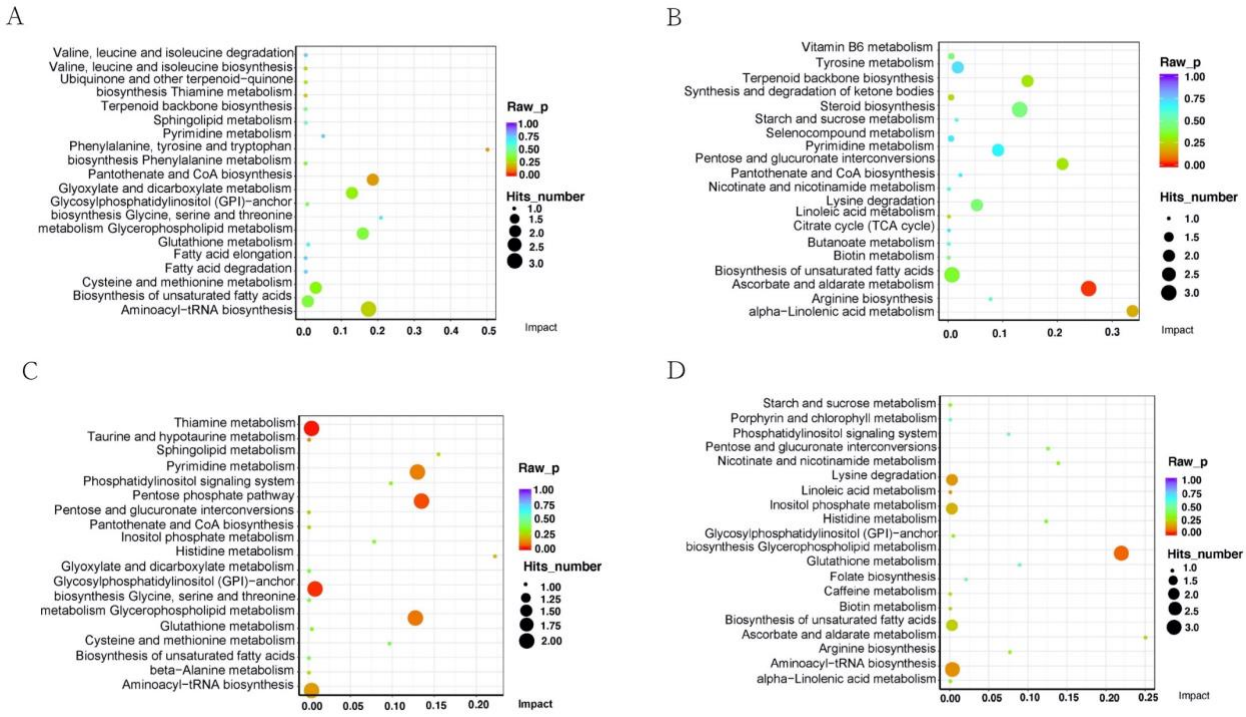

Figure 3. Statistics of pathway enrichment. (A) Differential metabolites between the CON and HS groups in the negative mode. (B) Differential metabolites between the CON and HS groups in the

positive mode. (C) Differential metabolites between the XBJ and HS groups in the negative mode. (D) Differential metabolites between the XBJ and HS groups in the positive mode.

518 **Tables**

519 Table 1 General indicators

Items	Group			SEM	P-value
	CON	HS	XBJ		
Body weight gain	12.02[a]	4.14[b]	7.32[a]	1.30	<0.05
Rectal temperature	35.35[b]	35.57[a]	35.47[b]	0.06	<0.05
LPS	363.8[c]	837.5[a]	535.3[b]	24.69	<0.05

520 Note: The superscript letters in each row of data indicate significant differences.

521

522 Table 2 Indicator of alpha diversity

523

Items	Group			P-value
	CON	HS	XBJ	
Chao1	752.74±21.51	645.10±30.03	750±33.02	0.74
Goods coverage	0.9956±0.00	0.9964±0.00	0.9959±0.00	0.44
Shannon	5.24±0.12	5.52±0.26	5.40±0.19	0.88
Simpson	0.87±0.01	0.92±0.01	0.90±0.01	0.37

530 Note: The results are presented as the means±SEM.

531

Figures

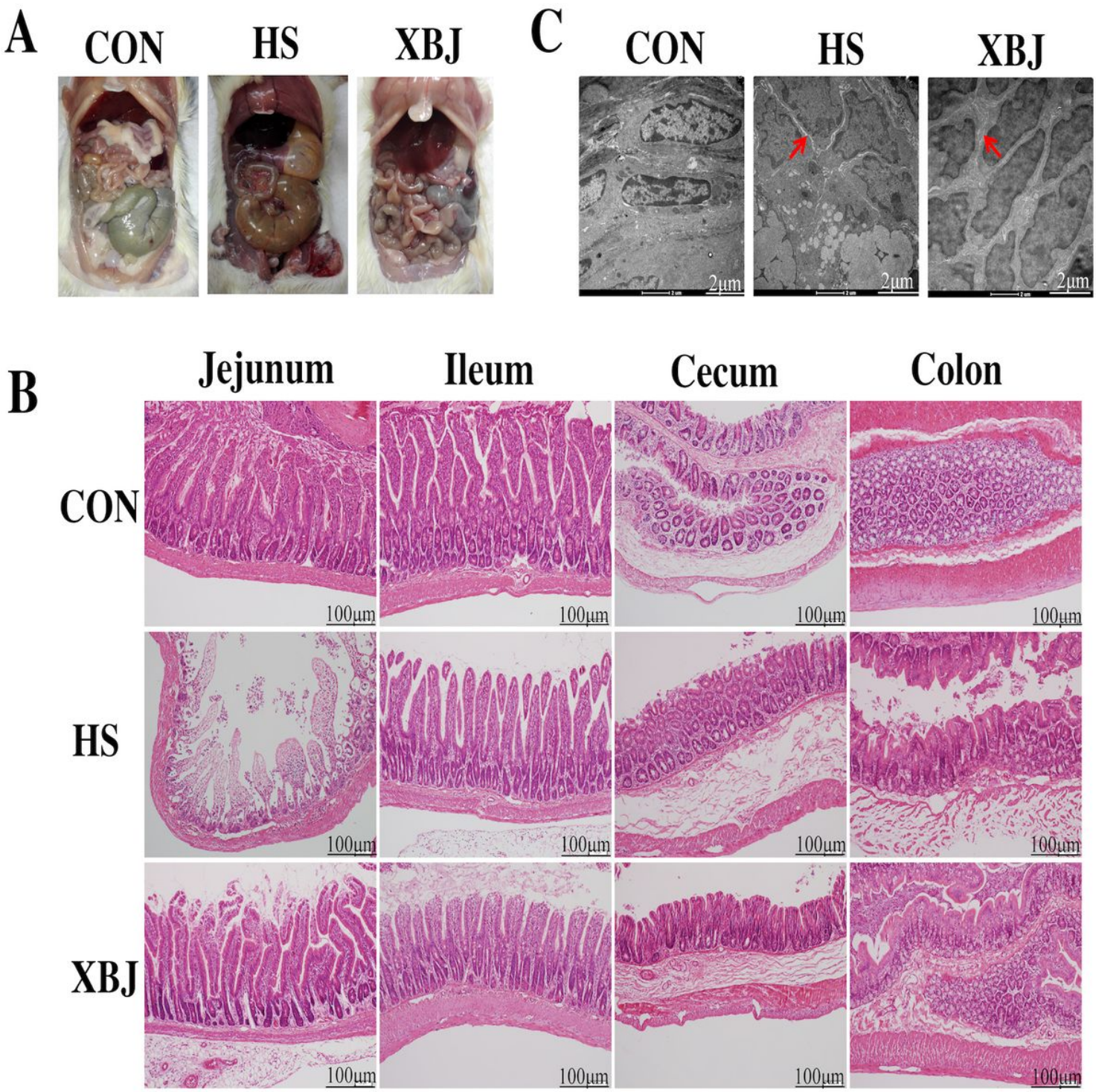

Figure 1

Intestinal structure. (A) Rat anatomy. (B) HE staining of different intestinal segments, including the jejunum, ileum, cecum and colon (40×). (C) Electron microscopy of the colon (8200×). Effect of XBJ on bacterial diversity in fecal microbiota

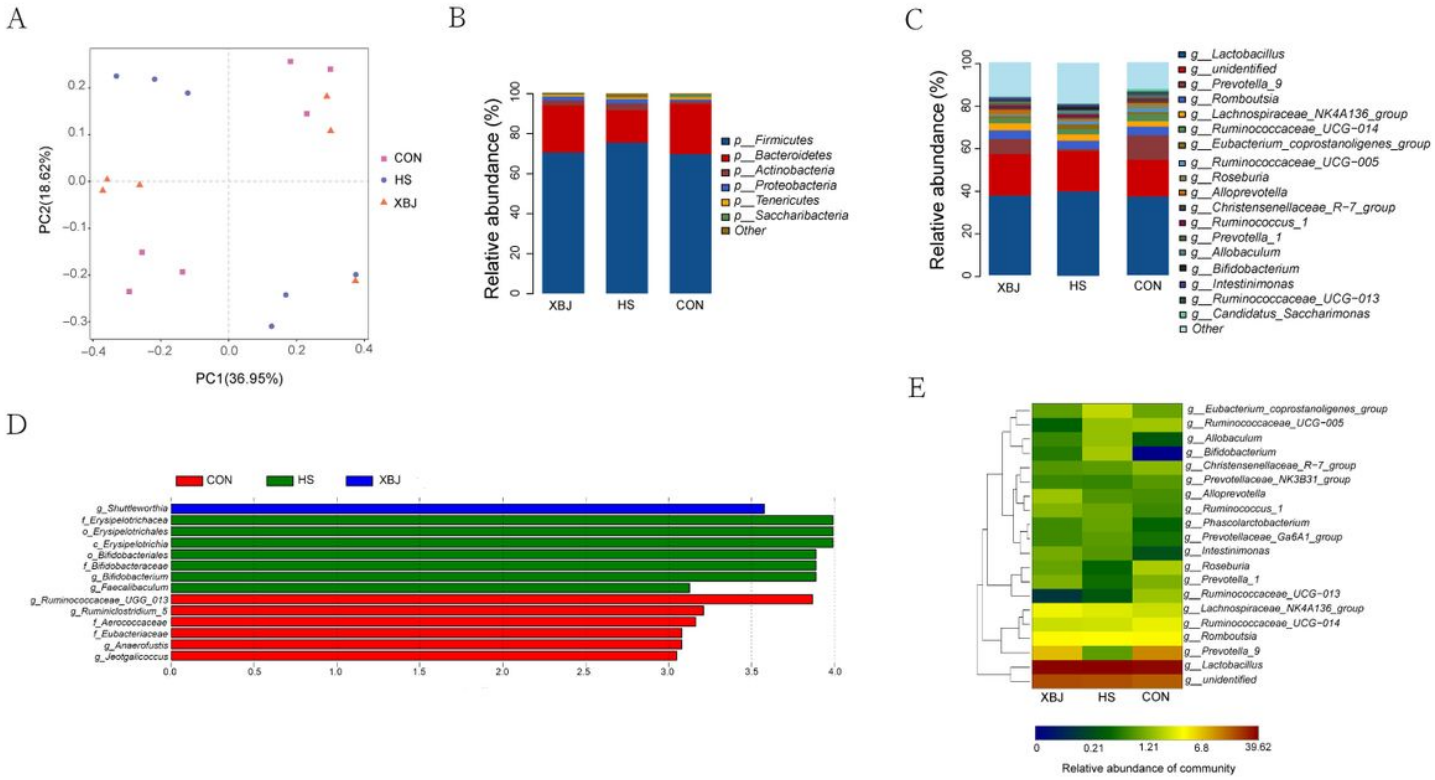

Figure 2

Intestinal microbiota. (A) Bray-Curtis PCoA plots. (B) Bar plot at the phylum level. (C) Bar plot at the genus level. (D) LEfSe score. (E) Heatmap at the genus level.

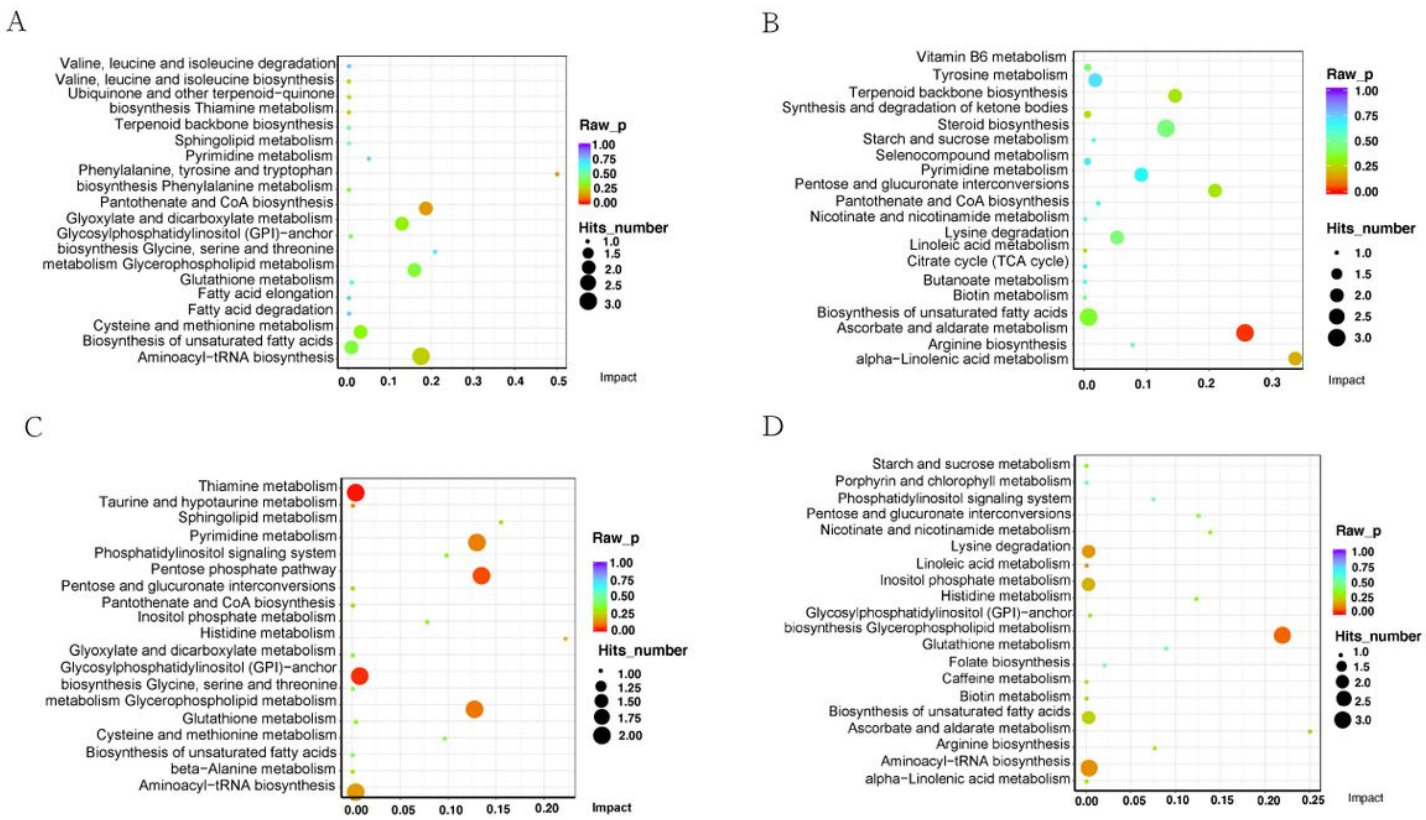

Figure 3

Statistics of pathway enrichment. (A) Differential metabolites between the CON and HS groups in the negative mode. (B) Differential metabolites between the CON and HS groups in the positive mode. (C) Differential metabolites between the XBJ and HS groups in the negative mode. (D) Differential metabolites between the XBJ and HS groups in the positive mode.

Supplementary Files

This is a list of supplementary files associated with this preprint. Click to download.

- Supplementary.pdf